Hindawi
International Journal of Antennas and Propagation
Volume 2019, Article ID 4264513, 14 pages
https://doi.org/10.1155/2019/4264513

Research Article

Wide CPW-Fed Multiband Wearable Monopole Antenna with Extended Grounds for GSM/WLAN/WiMAX Applications

Danvir Mandal[1] **and S. S. Pattnaik**[2]

[1]*I. K. Gujral Punjab Technical University, Kapurthala, 144603 Punjab, India*
[2]*National Institute of Technical Teachers Training and Research, Chandigarh 160019, India*

Correspondence should be addressed to Danvir Mandal; danvir.mandal@gmail.com

Received 23 May 2018; Revised 25 August 2018; Accepted 1 October 2018; Published 4 February 2019

Guest Editor: Mohammed M. Bait-Suwailam

A novel wide coplanar waveguide- (CPW-) fed multiband wearable monopole antenna is presented. The multiband operation is achieved by generating slanted monopoles of different lengths from an isosceles triangular patch. The different operating frequencies of the proposed antenna are associated with the lengths of the slanted monopoles, which are determined under quarter wavelength resonance condition. The CPW line is used as a multiband impedance-matching structure. The two grounds are slightly extended for better impedance matching. The proposed antenna is designed to cover the 1800 MHz GSM, 2.4 GHz/5.2 GHz WLAN, and 3.5 GHz WiMAX bands. The measured peak gains and impedance bandwidths are about 4.18/3.83/2.6/2.94 dBi and 410/260/170/520 MHz for the 1550-1960 MHz/2.3-2.56 GHz/3.4-3.57 GHz/5.0-5.52 GHz bands, respectively. The calculated averaged specific absorption rate (SAR) values at all the resonant frequencies are well below the standard limit of 2 W/kg, which ensures its feasibility for wearable applications. The antenna performance under different bending configurations is investigated and the results are presented. The reflection coefficient characteristics of the proposed antenna is also measured for different on-arm conditions and the results are compared. A good agreement between experimental and simulation results validates the proposed design approach.

1. Introduction

In today's world, for applications which involve wearable antennas, like health monitoring of patients and firefighting and military personal or body-centric communications, it becomes absolutely necessary that a single antenna operates on multiple bands, with SAR values well below the standard limits and its performance should not degrade under bent conditions. In order to satisfy these specific wireless communication requirements, multiband wearable antennas which can operate at 880–960 MHz/1710–1880 MHz for Global System for Mobile (GSM) communications, 2.4–2.484 GHz/5.15–5.825 GHz for wireless local area network (WLAN), and 3.4–3.69 GHz/5.25–5.85 GHz for Worldwide Interoperability for Microwave Access (WiMAX), are desired.

In the past few years, many single-, dual-, and multiband wearable antennas have been proposed [1–13]. In previous works, different methods have been used for designing single-band wearable antennas, such as antennas with an electromagnetic band gap (EBG) structure [1], antennas based on metamaterial structures [2, 3], monopole antennas fed by CPW [4], and electrotextile patch antennas [5]. Similarly, dual-band wearable antennas fed by CPW on a polypropylene substrate, polygon-shaped slotted wearable antennas on a jean substrate, wearable antennas using a metasurface, polyimide-based wearable antennas, and dual-mode textile antennas on a polydimethylsiloxane (PDMS) substrate have been reported in [6–10]. In [11–13], a multiband body-borne antenna for GSM/PCS/WLAN communications, a multiband wearable antenna using a metal rim, and a quad-band wearable slot antenna with low SAR values have been presented.

CPW-fed monopole antennas have been used frequently for the achievement of multiband operations [14–19]. CPW-fed dual-frequency monopole antennas have been presented in [14–16]. In [17], a three-band operation is achieved

in a CPW-fed slotted bow-tie monopole antenna. A multiband monopole antenna with double rectangular rings and vertical slots in the ground plane, fed by CPW, is reported in [18]. A CPW-fed three-band monopole antenna composed of a pentagonal radiating patch with two bent slots has been reported in [19].

The specific absorption rate of a wearable antenna should be calculated to ensure the safety of the user. Either single-layer or multilayer human head and human tissue models are used to calculate the specific absorption rate (SAR) of an antenna [1, 2, 7, 8, 10, 13, 20–23]. On the body performance of a wearable antenna, the investigation of its characteristics under bent conditions is very important. It is a well-established fact that the resonant frequency of a wearable antenna shifts under bending conditions. The on-arm performance and bending effect of a wearable antenna have been analyzed in [1–4, 7, 9, 10, 13, 24].

In this paper, we propose a four-band wearable monopole antenna fed by a wide CPW line. The small values of the substrate's dielectric constant increase the width of the CPW line. This limitation is exploited in this design. The proposed design has used the wide CPW line as a multiband impedance-matching structure. An isosceles triangular patch is slotted to generate four slanted monopoles for multiple wide-band operations. The antenna is tested under bent conditions and the results are presented. Antenna performance is also investigated for different on-arm conditions, with and without a cloth, and the results are compared. The specific absorption rate of the proposed antenna is found to be within standard limits. The geometrical structure and design procedure of the proposed antenna are presented in Section 2. Section 3 describes the simulation and measurement methodology. The results of the simulated and handmade proposed antenna are presented, compared, and analyzed in Section 4. The estimation of SAR values, effect of bending, and on-arm performance of the proposed antenna are also explained in this section. The paper is concluded in Section 5.

2. Antenna Geometry and Design Procedure

The geometry of the proposed multiband wearable antenna is shown in Figure 1. The antenna is formed by slanted monopoles using the approach applied in [17]. Generally, the planar quarter-wavelength monopoles have small bandwidths. To increase the bandwidth, taper-shaped elements are often used [17]. Hence, slanted monopoles are generated by slotting an isosceles triangular-shaped patch. The length of each monopole is set approximately equal to a quarter-wavelength of the desired resonant frequency. The length of each monopole is defined as

$$L_{mn} = \frac{\lambda_n}{4}, \tag{1}$$

where L_{mn} is the length and λ_n is the respective guided wavelength of the nth monopole. The antenna is fabricated on a polyester cloth substrate with 1 mm thickness, dielectric constant $\varepsilon_r = 1.39$, and loss tangent $\tan\delta = 0.01$ [3]. The thickness of the substrate is achieved by stitching

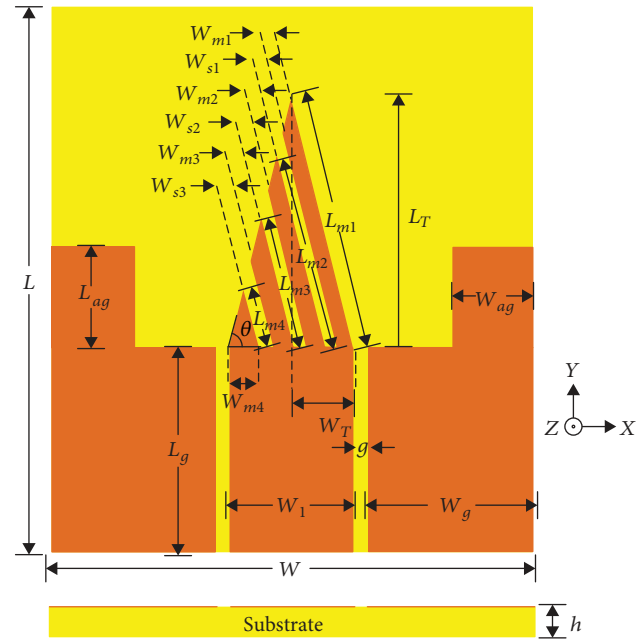

Figure 1: A wide CPW-fed multiband wearable monopole antenna with extended grounds.

multiple layers of the polyester cloth. The presence of an air gap between substrate layers can reduce the effective permittivity of the substrate. To eliminate the impact of the air gap, multiple layers of the polyester cloth are stitched in such a manner that they tightly adhered to each other leaving a negligible air gap.

The width of the CPW strip (W_1), gap (g), thickness (h), and dielectric constant (ε_r) of the substrate determine the effective dielectric constant (ε_{eff}) and characteristic impedance (Z_0) of the CPW line. The effective dielectric constant and characteristic impedance (Z_0) of a coplanar waveguide on a dielectric substrate of finite thickness [25] is given by

$$\varepsilon_{\text{eff}} = 1 + \frac{(\varepsilon_r - 1)}{2} \frac{K(k_1)}{K\left(k_1'\right)} \frac{K\left(k_0'\right)}{K(k_0)},$$
$$Z_0 = \frac{30\pi}{\sqrt{\varepsilon_{\text{eff}}}} \frac{K\left(k_0'\right)}{K(k_0)}, \tag{2}$$

where the modulus of the complete elliptic integrals of the first kind $K(k_0)$, $K(k_0')$, $K(k_1)$, and $K(k_1')$ are as follows:

$$k_0 = \frac{W_1}{W_1 + 2g},$$
$$k_0' = \sqrt{1 - k_0^2},$$
$$k_1 = \frac{\sinh(\pi W_1/4h)}{\sinh\{[\pi(W_1 + 2g)]/4h\}}, \tag{3}$$
$$k_1' = \sqrt{1 - k_1^2}.$$

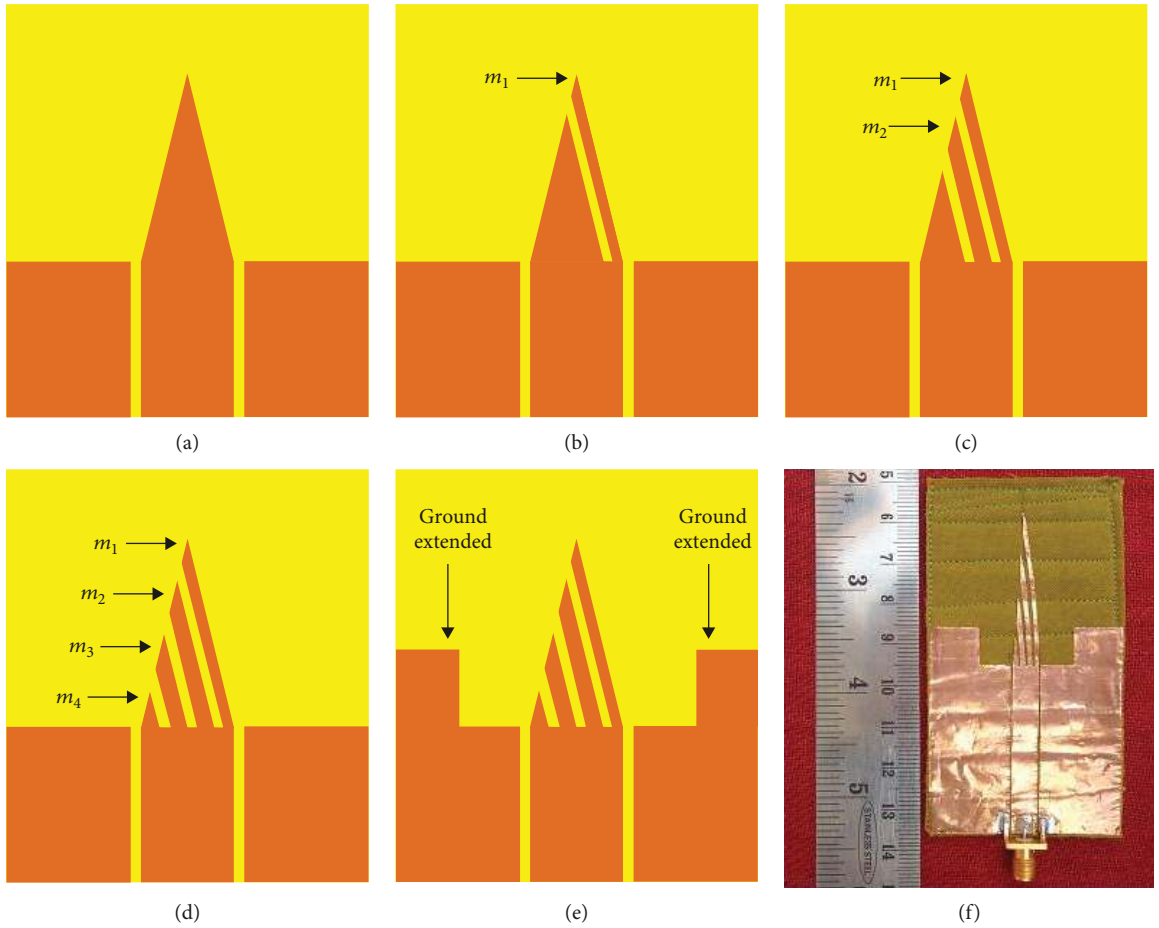

FIGURE 2: Geometries of (a) Antenna I, (b) Antenna II, (c) Antenna III, (d) Antenna IV, and (e) Antenna V and (f) photograph of the proposed handmade Antenna V.

The size of the proposed antenna considering the substrate size is $45.5 \times 85 \times 1$ mm^3. The design procedure of the antenna, which consists of five steps, is elaborated and shown in Figure 2.

Step 1. Initially, a CPW-fed triangular patch with parameters $L = 85.0$ mm, $W = 45.5$ mm, $L_g = 40.0$ mm, $W_g = 19.4$ mm, $L_T = 38.5$ mm, $W_T = 3.15$ mm, $W_1 = 6.3$ mm, $g = 0.2$ mm, and $\theta = 85.5^\circ$ is designed. This wide CPW-fed triangular patch wearable antenna is designated Antenna I as shown in Figure 2(a). The effective dielectric constant for this design is $\varepsilon_{\text{eff}} = 1.13$.

Step 2. The first slanted monopole m_1 at a resonant frequency of 1800 MHz is generated by slotting the triangular patch. The theoretical length of the slanted monopole m_1 under quarter-wavelength resonance condition is 39.19 mm. The length L_T and width W_T of the triangular patch is taken to match the length L_{m1} of the first slanted monopole m_1, which is given by

$$L_{m1} = \left(L_T^2 + W_T^2\right)^{0.5}. \tag{4}$$

For the selected length L_T and width W_T of the isosceles triangular patch, the value of θ comes out to be approximately 85.5°, which is estimated as

$$\theta = \sin^{-1} \frac{L_T}{L_{m1}}. \tag{5}$$

Due to the mutual coupling between the slanted monopole m_1 and the rest of the triangular patch which affects the resonant frequency, the final length L_{m1} of the slanted monopole m_1 is modified to be 38.62 mm. The width W_{m1} of the first slanted monopole m_1 is 1.0 mm. This slanted monopole with the remaining triangular patch is denoted Antenna II. It is shown in Figure 2(b). The width W_{s1} of the first slot is 0.4 mm. It is considered in such a way to match the length of the second monopole m_2.

Step 3. The second slanted monopole m_2 at a resonant frequency of 2.4 GHz is generated by making another slot in the remaining triangular patch. Theoretically, the quarter wavelength at 2.4 GHz is 29.39 mm, whereas practically, the length L_{m2} of the slanted monopole m_2 is kept at 30.45 mm with a width W_{m2} of 1.2 mm. Two slanted monopoles m_1 and m_2 along with the remaining triangular patch as shown

in Figure 2(c) is designated Antenna III. The width W_{s2} of the second slot is 0.35 mm. It is considered to match the length of the third monopole m_3.

Step 4. The third slot with a width of $W_{s3} = 0.45$ mm is cut in a triangular patch to generate the third slanted monopole m_3 at a resonant frequency of 3.5 GHz. The quarter wavelength at 3.5 GHz is 20.15 mm. The final length L_{m3} of the third slanted monopole m_3 is kept at 20.53 mm with a width W_{m3} of 1.5 mm. This antenna with three monopoles and the remaining triangular patch is designated Antenna IV as shown in Figure 2(d). The remaining triangular patch is the fourth monopole which resonates at 5.38 GHz. The length L_{m4} and width W_{m4} of this fourth monopole is 8.578 mm and 1.4 mm, respectively.

Step 5. In the case of Antenna IV, the reflection coefficient and bandwidth of the four bands at 1800 MHz, 2.4 GHz, 3.5 GHz, and 5.38 GHz are not adequate and need to be improved. To improve the reflection coefficient and bandwidth of the four bands, both ground patches are extended with length L_{ag} and width W_{ag}. The required four-band operation is obtained when $L_{ag} = 9$ mm and $W_{ag} = 12$ mm. These extended grounds provided voltage standing wave ratio (VSWR) values close to 1 at four resonating frequencies, which proves improved impedance matching. Improved impedance matching further decreases the reflection coefficient and increases the bandwidth of the four respective bands. The antenna with four monopoles along with extended grounds is the final required design denoted Antenna V. Antenna V is shown in Figure 2(e). The photograph of the handmade Antenna V is shown in Figure 2(f).

3. Simulation and Measurement Methodology

The antenna design is simulated using a high-frequency structure simulator (HFSS). The simulation is performed for the reflection coefficients (S_{11}) of the proposed antenna with varying L_{ag} and W_{ag}, for 3-dimensional and 2-dimensional radiation patterns, gain, radiation efficiency, surface current density distribution, and SAR values at all resonant frequencies. The reflection coefficient (S_{11}) of the handmade Antenna V is measured using the ANRITSU MS46322A vector network analyzer. The expression used to measure the gain of the Antenna V is given as [13] follows:

$$\text{Gain of the test antenna} = G + (P_T - P_R), \tag{6}$$

where G is the gain of the reference pyramidal horn antenna known over the anisotropic antenna, P_T and P_R are the power received by the test antenna and the power received by the reference antenna, respectively.

A three-layer human tissue model is used for the estimation of SAR values at the measured resonant frequencies of the proposed antenna. The permittivity (ε_r) and conductivity σ (S/m) of the skin (dry and wet), fat, and muscle layers at 1780 MHz, 2.40 GHz, 3.46 GHz, and 5.26 GHz are listed in Tables 1 and 2 [7, 13, 23, 26]. The thickness, mass density, and loss tangent [7] of the skin, fat, and muscle layers are summarized in Table 3. The surface size of the human tissue model used for SAR calculations is 200×200 mm^2. The IEEE C95.3 standard, in which SAR is averaged over 10 g of biological tissue, is used to calculate averaged SAR [2, 13].

Table 1: Permittivity (ε_r) of skin, fat, and muscle.

Layer	Permittivity (ε_r)			
	1780 MHz	2.40 GHz	3.46 GHz	5.26 GHz
Skin (dry)	38.90	38.06	37.04	35.56
Skin (wet)	43.88	42.92	41.53	39.30
Fat	5.35	5.28	5.17	5.00
Muscle	54.47	53.63	52.25	49.77

Table 2: Conductivity σ (S/m) of skin, fat, and muscle.

Layer	Conductivity σ (S/m)			
	1780 MHz	2.40 GHz	3.46 GHz	5.26 GHz
Skin (dry)	1.17	1.44	1.99	3.25
Skin (wet)	1.22	1.56	2.27	3.80
Fat	0.07	0.10	0.15	0.25
Muscle	1.37	1.77	2.62	4.53

Table 3: Thickness, density, and loss tangent of skin, fat, and muscle layers.

Layer	Thickness (mm)	Density (kg/m^3)	Loss tangent
Skin	3	1090	0.418
Fat	10	1100	0.186
Muscle	30	1050	0.342

In order to investigate the effects of slight and severe bending on antenna performance, two diameters have been taken for bending analysis. The 160 mm diameter offers slight bending, while the 110 mm diameter offers severe bending. The reflection coefficients (S_{11}) of the proposed antenna have been measured for light and severe bending configurations along x and y planes, and are compared with simulation results. Two on-arm conditions, with and without cloth, have been used to measure the performance of the proposed antenna on human body.

4. Results and Discussion

The simulated reflection coefficients (S_{11}) of Antenna I to Antenna V are summarized in Figure 3. The effect of L_{ag} and W_{ag} on the overall reflection coefficient (S_{11}) is illustrated in Figures 4 and 5. Antenna I covers two bands from 1840 MHz to 2400 MHz (560 MHz, 26.42%) and 5.4 GHz to 6.3 GHz (900 MHz, 15.38%).

Antenna II has three bands that cover from 1660 MHz to 1920 MHz (260 MHz, 14.53%), 2.52 GHz to 2.7 GHz (180 MHz, 8.34%), and 5.2 GHz to 5.8 GHz (600 MHz, 10.9%). Antenna III covers three bands from 1660 MHz to 1960 MHz (300 MHz, 16.57%), 2.36 to 2.46 GHz (100 MHz, 4.15%), and 5.3 GHz to 5.84 GHz (540 MHz, 9.69%).

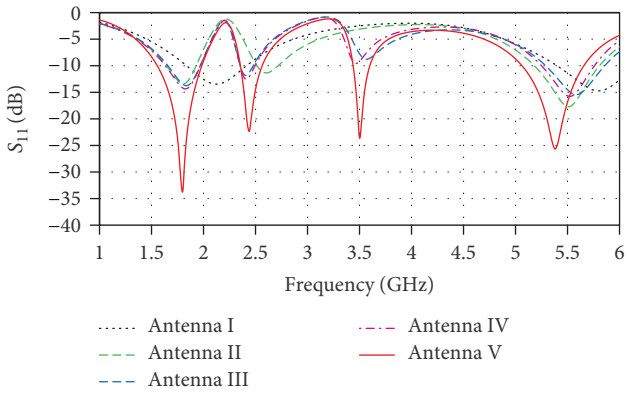

Figure 3: Simulated reflection coefficient (S_{11}) of Antenna I to Antenna V.

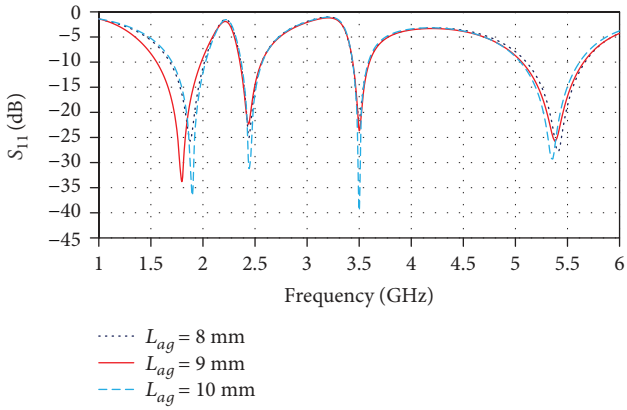

Figure 4: Reflection coefficient (S_{11}) of Antenna V at W_{ag} = 12 mm and L_{ag} = 8, 9, and 10 mm.

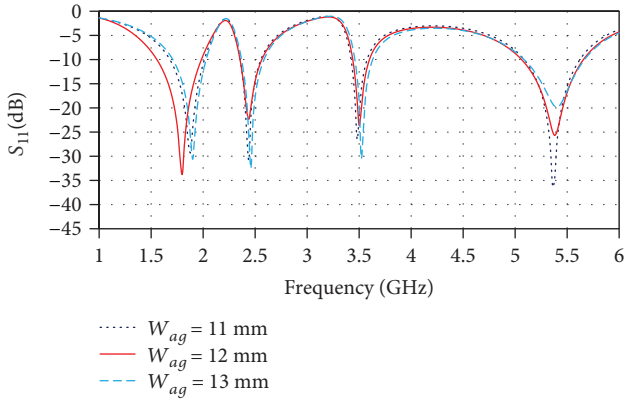

Figure 5: Reflection coefficient (S_{11}) of Antenna V at L_{ag} = 9 mm and W_{ag} = 11, 12, and 13 mm.

Antenna IV has three bands that cover from 1640 MHz to 1960 MHz (320 MHz, 17.78%), 2.36 GHz to 2.48 GHz (120 MHz, 4.96%), and 5.26 GHz to 5.74 GHz (480 MHz, 8.73%). Antenna V covers four required bands from 1550 MHz to 1980 MHz (430 MHz, 24.36%), 2.36 GHz to 2.56 GHz (200 MHz, 8.13%), 3.43 GHz to 3.59 GHz (160 MHz, 4.56%), and 5.08 GHz to 5.65 GHz (570 MHz, 10.62%). The resonant frequencies of the simulated Antenna V are 1800 MHz, 2.44 GHz, 3.5 GHz, and 5.38 GHz, with reflection coefficient values of −33.7 dB, −22.3 dB, −23.6 dB, and −25.6 dB, respectively.

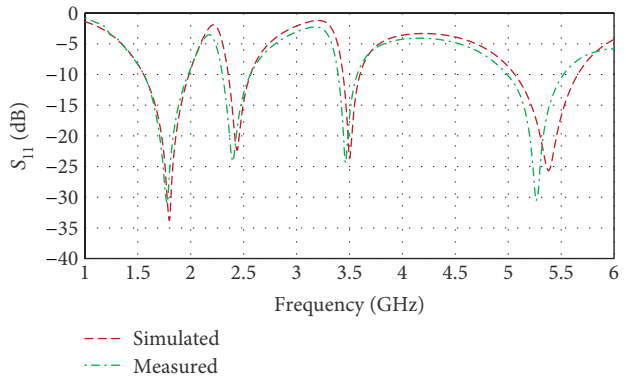

Figure 6: Measured and simulated reflection coefficient of Antenna V.

The first band of Antenna V covers the 1710–1880 MHz GSM band. The second band of Antenna V satisfies the requirement of 2.4–2.484 GHz WLAN applications. The third band of Antenna V operates within the 3.4–3.7 GHz WiMAX range. The fourth band of Antenna V covers the 5.15–5.35 GHz WLAN operational band. Figure 6 shows the measured and simulated reflection coefficients of Antenna V.

The measured operating bands of Antenna V are 1550 MHz to 1960 MHz (410 MHz, 23.36%), 2.3 GHz to 2.56 GHz (260 MHz, 10.69%), 3.4 GHz to 3.57 GHz (170 MHz, 4.87%), and 5.0 GHz to 5.52 GHz (520 MHz, 9.89%). The measured resonant frequencies of Antenna V are 1780 MHz, 2.40 GHz, 3.46 GHz, and 5.26 GHz, with reflection coefficient values of −30.8 dB, −24.15 dB, −24.3 dB, and −30.4 dB, respectively.

From the simulated and measured results, a slight shift in the resonant frequencies accompanied by a change in reflection coefficient values has been found. This can be attributed to the inconsistency in the fabrication process and soldering tolerance.

Refereeing to these results, the proposed antenna can satisfy the 1800 MHz GSM, 2.4/5.2 GHz WLAN, and 3.5 GHz WiMAX bands, resulting in a four-band operation.

Figure 7 shows the surface current distributions of Antenna V at 1800 MHz, 2.44 GHz, 3.5 GHz, and 5.38 GHz. The surface current densities are at the maximum in the corresponding monopoles at the respective simulated resonant frequencies of 1800 MHz, 2.44 GHz, 3.5 GHz and 5.38 GHz. In monopole elements that are sufficiently thin electrically and not too long, the element current distribution is approximately sinusoidal [27]. The first quarter-wavelength monopole m_1 corresponding to 1800 MHz is the thinnest among all four monopoles, and its current distribution is nearly sinusoidal.

Since the measured resonant frequencies of Antenna V are 1780 MHz, 2.40 GHz, 3.46 GHz, and 5.26 GHz, Figure 8 shows the 3-dimensional simulated radiation patterns of Antenna V at measured resonant frequencies. Figures 9–12

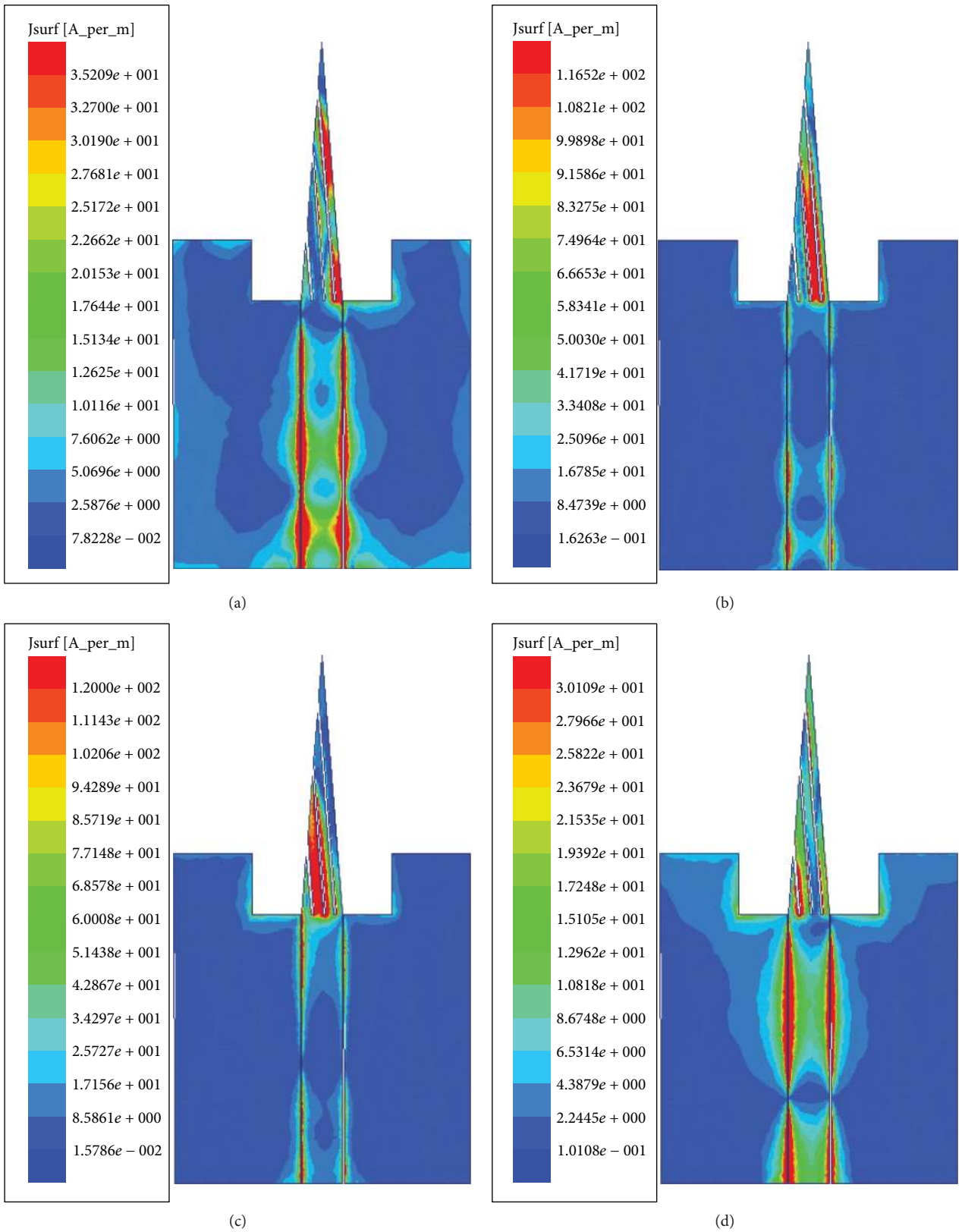

Figure 7: Surface current density distributions of Antenna V at (a) 1800 MHz, (b) 2.44 GHz, (c) 3.5 GHz, and (d) 5.38 GHz.

illustrate the 2-dimensional simulated and measured radiation patterns in x–z, y–z, and x–y planes of Antenna V at measured resonant frequencies.

CPW-fed antennas normally suffer backward radiation. The radiation patterns at 1780 MHz and 2.4 GHz are quite similar and also suffered backward radiation, which is the

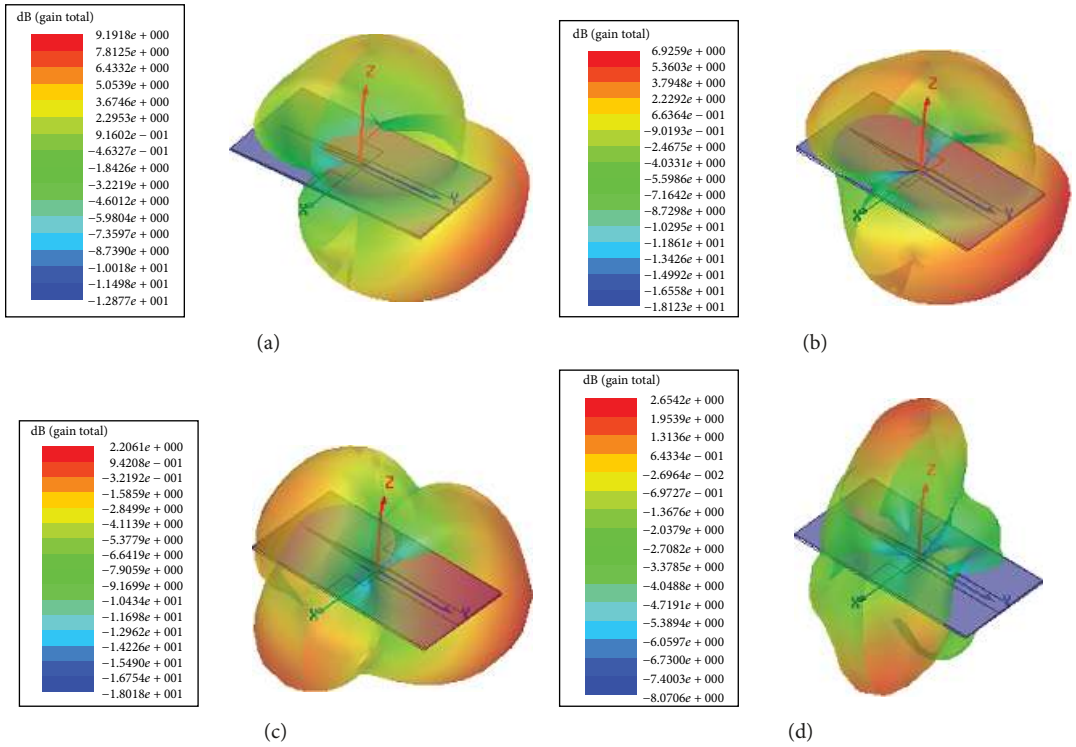

Figure 8: 3-Dimensional simulated radiation patterns of Antenna V at (a) 1780 MHz, (b) 2.40 GHz, (c) 3.46 GHz, and (d) 5.26 GHz.

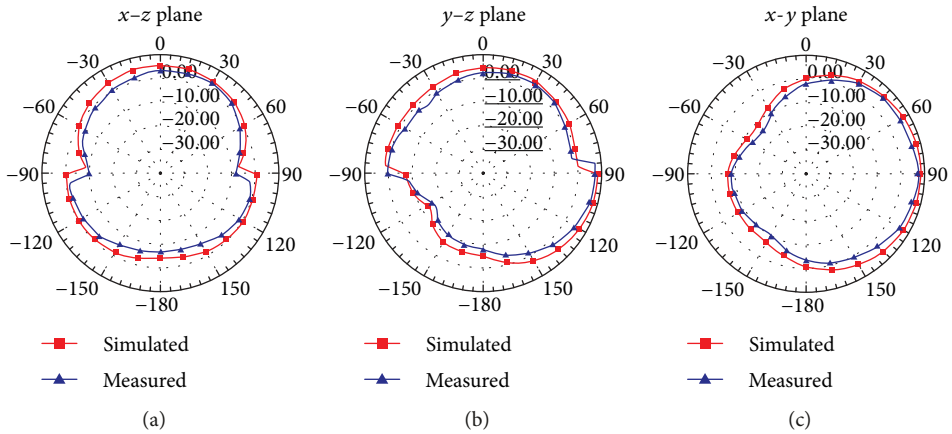

Figure 9: 2-Dimensional simulated and measured radiation patterns of Antenna V at 1780 MHz.

reason for the shapes of their radiation patterns. However, at 3.46 GHz and 5.26 GHz, the radiation patterns are distinct.

Figure 13 shows the measured and simulated peak gains versus the frequency of Antenna V. The measured and simulated peak gains in the 1550–1960 MHz band vary from 3.3 to 4.18 dBi and 8.51 to 9.33 dB, respectively. The measured and simulated results in the 2.3–2.56 GHz band described that the gain variations are from 3.24 to 3.83 dBi and 5.63 to 7.15 dB. For the third and fourth operating bands of 3.4–3.57 GHz and 5.0–5.52 GHz, the measured peak gains are about 1.86–2.6 dBi and 2.01–2.94 dBi. The simulated peak gains for the 3.4–3.57 GHz and 5.0–5.52 GHz bands lie within 1.74 to 2.41 dB and 1.59 dB to 2.75 dB, respectively. The simulated radiation efficiency of the proposed Antenna V is shown in Figure 14. For the 1550 MHz–1960 MHz band, the radiation efficiency is about 91.92 to 94.94%. In the second band of 2.3–2.56 GHz, the radiation efficiency varies from 82.16 to 95.69%.

The results in the 3.4–3.57 GHz and 5.0–5.52 GHz bands described that the radiation efficiency variations are from 80.89 to 94.10% and 80.20 to 87.82%, respectively.

4.1. Specific Absorption Rate (SAR) Estimation. Figure 15 shows the three-layer human tissue model [13] used for SAR calculations at the measured resonant frequencies of Antenna V. The estimated SAR values for dry and wet skin are investigated and the results are compared in Table 4.

Referring to these results, SAR values tend to increase with an increase in the simulating frequency of the human tissue model except at 5.26 GHz. It is due to the pointed

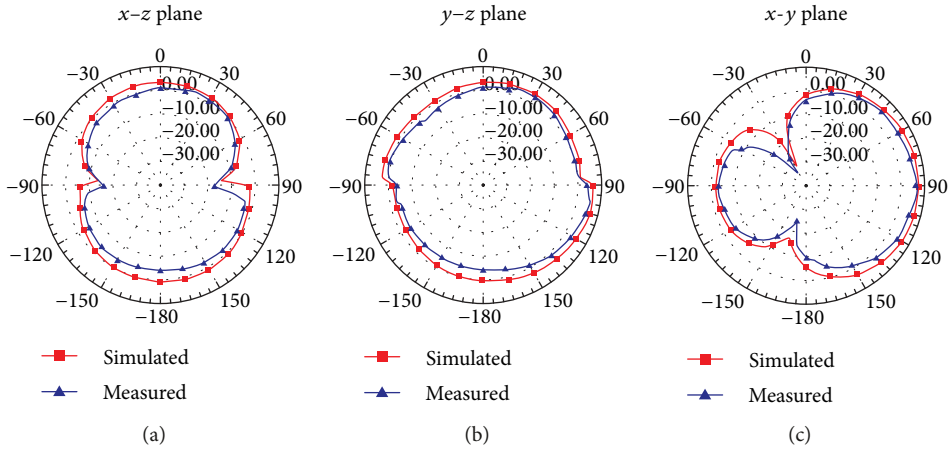

Figure 10: 2-Dimensional simulated and measured radiation patterns of Antenna V at 2.40 GHz.

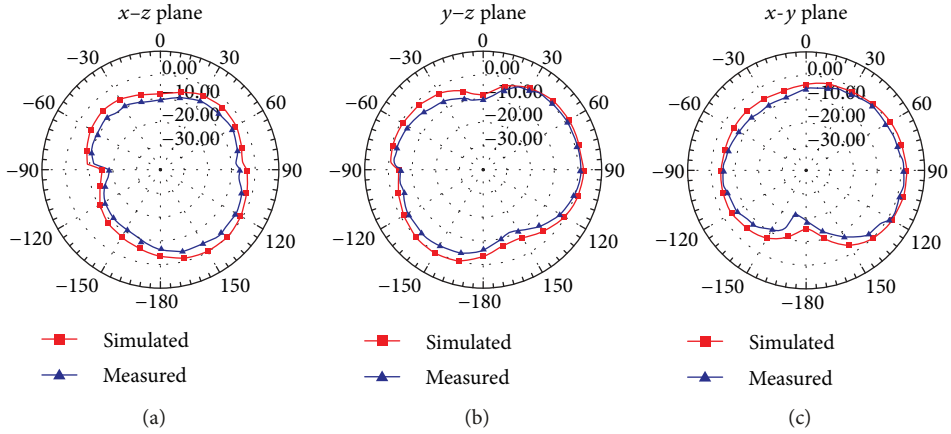

Figure 11: 2-Dimensional simulated and measured radiation patterns of Antenna V at 3.46 GHz.

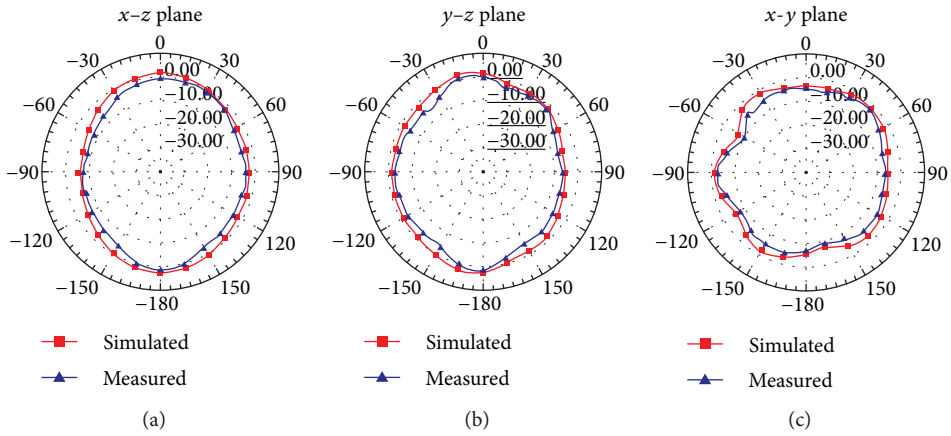

Figure 12: 2-Dimensional simulated and measured radiation patterns of Antenna V at 5.26 GHz.

radiation pattern in the z direction at 5.26 GHz, which shows that a small amount of radiation is illuminating the human tissue model, and therefore, the reason for the low SAR value at 5.26 GHz.

The estimated SAR value for the human tissue model with wet skin is higher than that of the model with dry skin for 1780 MHz, whereas for 2.4 GHz, 3.46 GHz, and 5.26 GHz, the SAR values for the model with dry skin are higher than that of the model with wet skin.

4.2. Antenna Performance under Bending Configurations. Bending is investigated in the x and y planes by keeping the handmade Antenna V around the PVC (polyvinyl chloride) pipes [3, 13] with diameters of 160 mm and 110 mm as

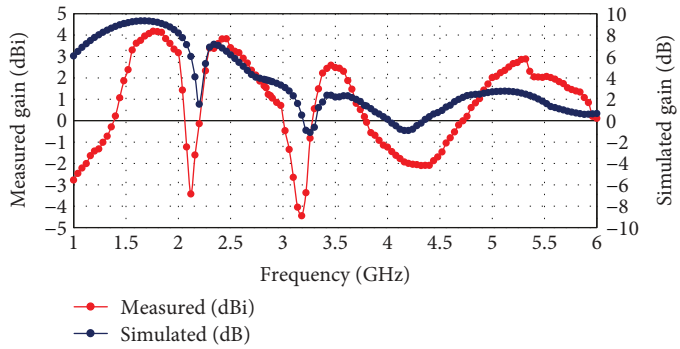

Figure 13: Measured and simulated peak gain of the proposed Antenna V.

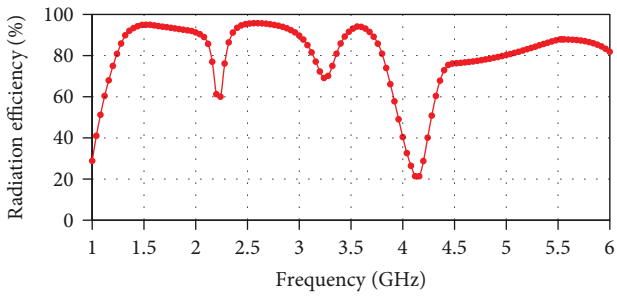

Figure 14: Radiation efficiency of the proposed Antenna V.

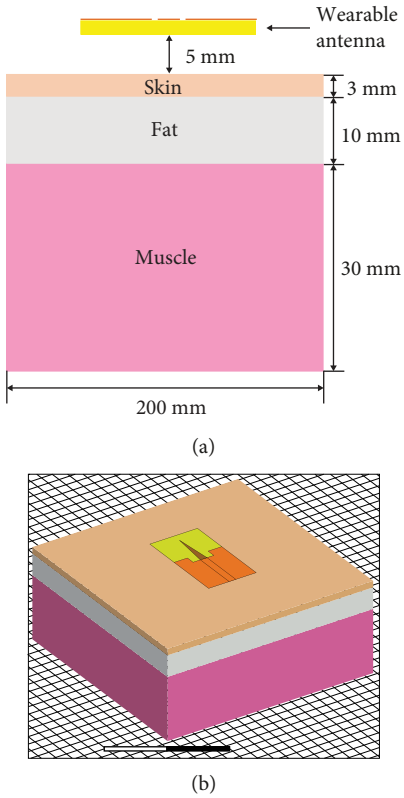

Figure 15: Modelling of (a) Antenna V on a three-layer human tissue model for SAR calculation and (b) Antenna V over a three-layer human tissue model in HFSS [13] (reproduced courtesy of the Electromagnetics Academy).

Table 4: Estimated SAR (W/kg) values for the three-layer human tissue model with dry and wet skin.

Frequency	Average SAR (W/kg)	
	Dry skin	Wet skin
1780 MHz	0.2293	0.2549
2.40 GHz	0.3892	0.3861
3.46 GHz	0.4640	0.4447
5.26 GHz	0.2535	0.2512

shown in Figure 16. Figure 17 shows the four cases of bending during HFSS simulation.

Figures 18–21 compare the measured reflection coefficient of the flat Antenna V in free space with the simulated and measured reflection coefficients of Antenna V, bent along the x and y planes on PVC pipes with radii of 55 mm and 80 mm. Frequency detuning, which is observed when simulated and measured results are compared for all four cases of the bending of Antenna V, is presented in Table 5.

For both simulated and measured results, the 1780 MHz band shifts to the right side of the spectrum for all four bending cases of Antenna V. Similarly, in the case of the simulated results, the 2.4 GHz band shifts to the right side of the spectrum for all four cases of bending of Antenna V along the x and y planes. The measured results described that the 2.4 GHz band shifts to the right side of the spectrum for Cases 2 and 3, but it does not shift for Cases 1 and 4.

The simulated results of the four bending cases illustrated that the 3.46 GHz band shifts to the left side for Cases 1, 3, and 4, whereas it shifts to the right side of the spectrum for Case 2. However, the measured results show that the 3.46 GHz band shifts to the left side for Cases 1 and 3, does not shift for Case 2, and shifts to the right side of the spectrum for Case 4.

The simulated as well as measured results show that the last 5.26 GHz band shifts to the left side of the spectrum for all four bending cases of Antenna V. In our proposed antenna, it could be easily seen that the antenna has strong currents on its ground planes, especially around the CPW feed line. The ground planes are actually a part of the proposed CPW-fed antenna. Taking this into account, it could be deduced that the distribution of the currents in the ground plane will change with the size and or/shape of the ground plane. As a result, the impedance and radiation performance

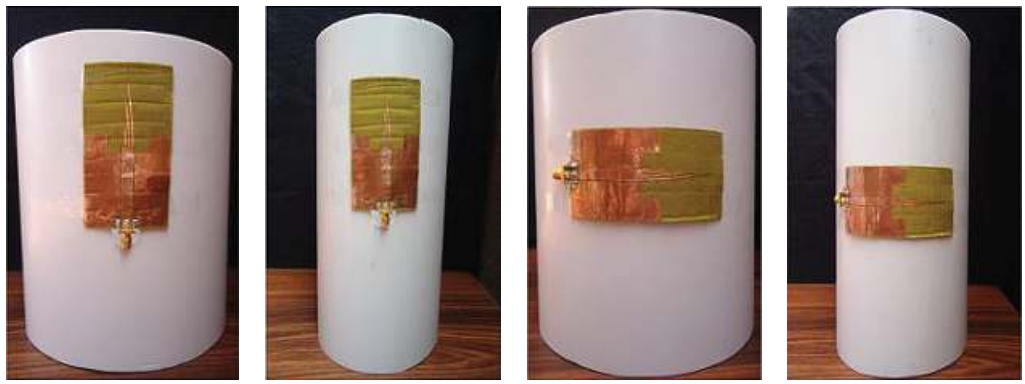

(a) (b) (c) (d)

Figure 16: Photographs of Antenna V under four bending conditions on a PVC pipe (a) bent along the x plane on an 80 mm radius, (b) bent along the x plane on a 55 mm radius, (c) bent along the y plane on an 80 mm radius, and (d) bent along the y plane on a 55 mm radius.

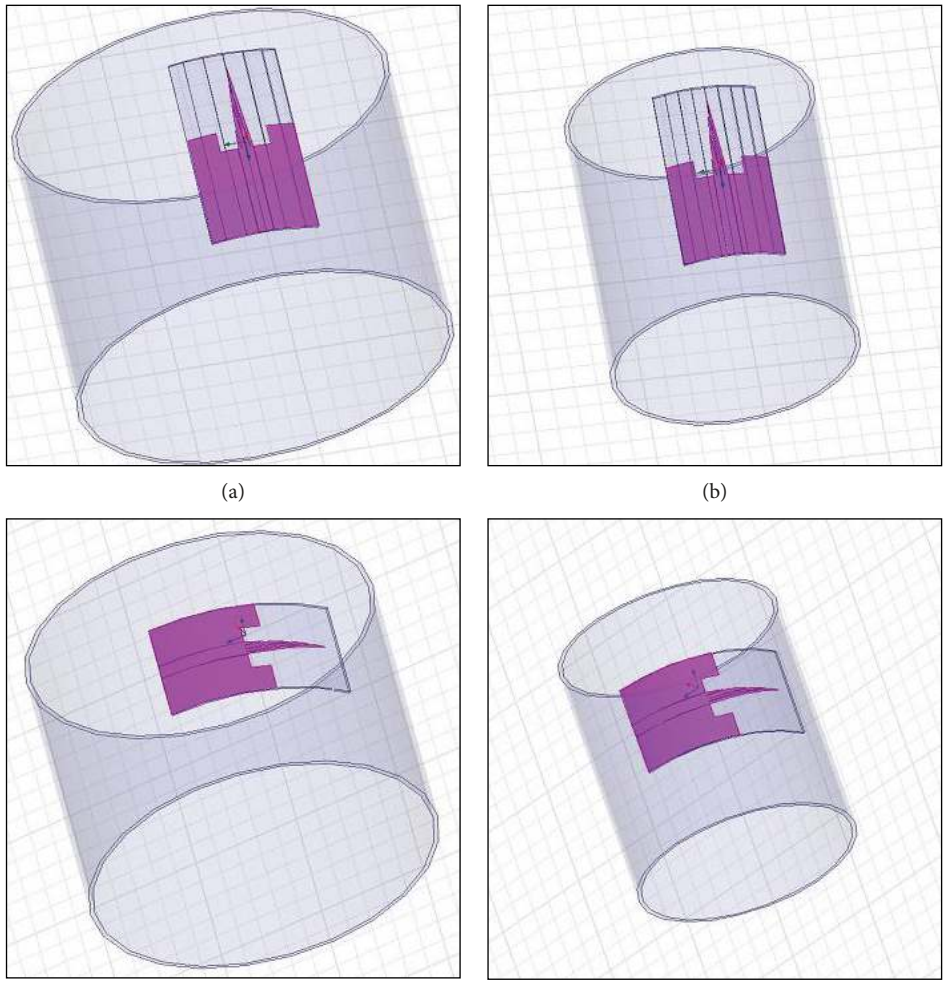

(a) (b) (c) (d)

Figure 17: HFSS simulation photographs of Antenna V under four bending conditions on a PVC pipe (a) bent along the x plane on an 80 mm radius, (b) bent along the x plane on a 55 mm radius, (c) bent along the y plane on an 80 mm radius, and (d) bent along the y plane on a 55 mm radius.

of the antenna will change, similar to that in [6]. The bending of Antenna V along the x plane has more effects on ground planes, giving rise to an impedance mismatch, which is more significant for the 3.46 GHz band. This band is also severely degraded during bending along the x plane, for both the 55 mm and 80 mm bending radius cases. Similarly, the

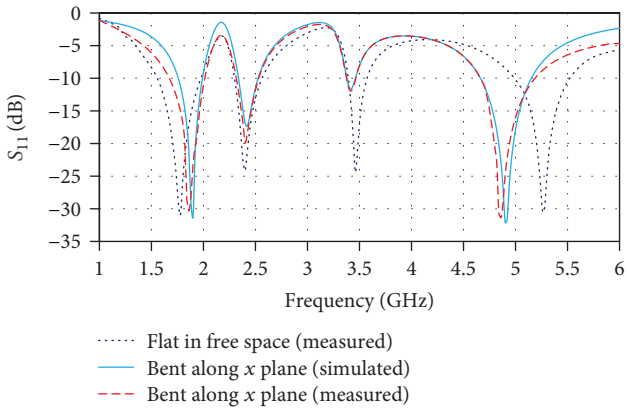

FIGURE 18: Simulated and measured reflection coefficients of Antenna V bent along the x plane on a PVC pipe with an 80 mm radius.

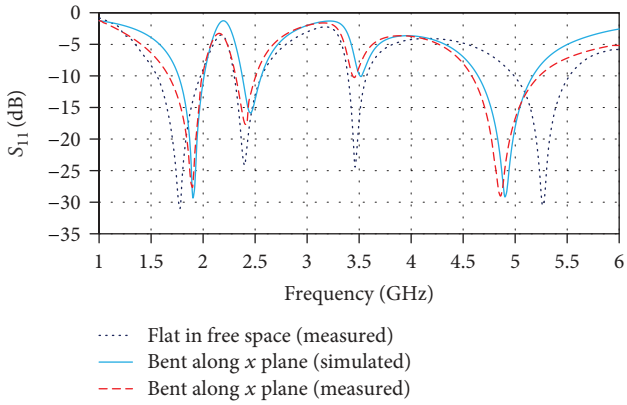

FIGURE 19: Simulated and measured reflection coefficients of Antenna V bent along the x plane on a PVC pipe with a 55 mm radius.

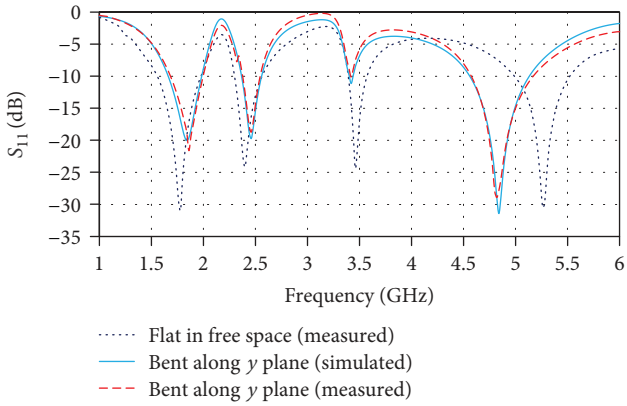

FIGURE 20: Simulated and measured reflection coefficients of Antenna V bent along the y plane on a PVC pipe with an 80 mm radius.

bending of Antenna V along the y plane changed the electrical length of the antenna and CPW line, which again increases the impedance mismatch of the proposed antenna,

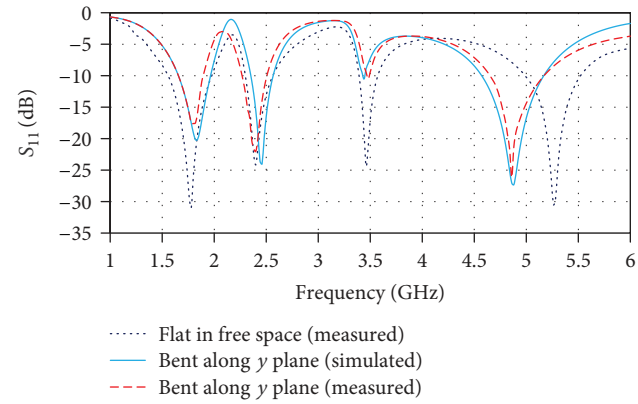

FIGURE 21: Simulated and measured reflection coefficients of Antenna V bent along the y plane on a PVC pipe with a 55 mm radius.

especially for the 3.46 GHz band, degrading it for both the 55 mm and 80 mm bending radius cases.

For bending along the x plane, the measured and simulated frequency detuning values of Case 2 are either equal to or higher than that of Case 1, except for the 3.46 GHz band, for the measured value. On the contrary, for bending along the y plane, the measured and simulated frequency detuning values of Case 4 are either equal to or less than that of Case 3.

Maximum frequency detuning is observed for Case 3 at the 5.26 GHz band. In the measured results of the 2.4 GHz and 3.46 GHz bands, no frequency shift is observed for Cases 1, 4, and 2, respectively. Minimum frequency detuning has been found at the 3.46 GHz band for Case 4.

4.3. On-Arm Performance of the Proposed Antenna. Figure 22 illustrates the setup for two on-arm conditions of Antenna V during reflection coefficient measurement. The first condition is Antenna V on arm, without cloth, and the second condition is Antenna V on arm, with cloth [13, 24].

The measured reflection coefficients for the two on-arm conditions are compared with the measured reflection coefficient of the flat Antenna V in free space, and the results are presented in Figure 23. For both on-arm conditions, the 1780 MHz, 2.4 GHz, and 3.46 GHz bands shifted to the left side, whereas the 5.26 GHz band shifted to the right side of the spectrum. The reflection coefficient of all bands of Antenna V for the on-arm, without-cloth condition, decreases.

For the on-arm, with-cloth condition, the reflection coefficient of the 1780 MHz and 5.26 GHz bands decreases, while that of 2.4 GHz band increases and that of 3.46 GHz band remains unchanged.

The frequency detuning of Antenna V for the two on-arm conditions is given in Table 6. The frequency detuning values of Antenna V for the on-arm, without-cloth condition are higher than that for the on-arm, with-cloth condition.

Maximum frequency detuning is calculated at the 1780 MHz band for the without-cloth condition during on-arm performance measurements. Minimum frequency

Table 5: Frequency detuning of Antenna V for bending in the x and y planes.

Resonant frequency	Simulated/measured	Frequency detuning (%)			
		x plane		y plane	
		Case 1 80 mm bending radius	Case 2 55 mm bending radius	Case 3 80 mm bending radius	Case 4 55 mm bending radius
1780 MHz	Simulated	6.74	6.74	3.37	2.24
	Measured	4.49	6.74	4.49	1.12
2.4 GHz	Simulated	0.83	2.50	2.50	2.50
	Measured	0.00	0.83	2.50	0.00
3.46 GHz	Simulated	1.15	1.73	1.15	0.57
	Measured	1.15	0.00	1.15	0.57
5.26 GHz	Simulated	6.84	6.84	7.98	7.22
	Measured	7.60	7.60	8.36	7.60

(a) (b)

Figure 22: Setup for performance measurement of Antenna V for on-arm (a) without-cloth and (b) with-cloth conditions.

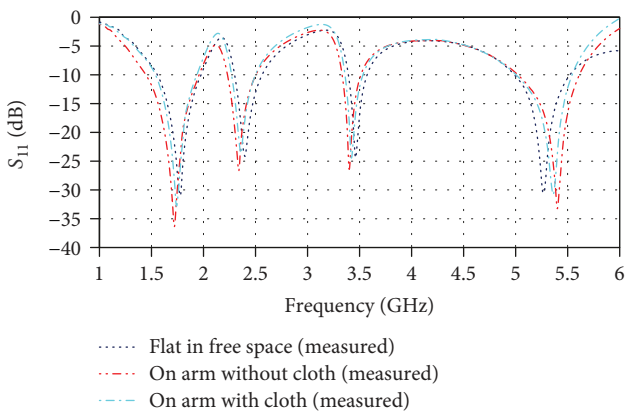

Figure 23: Measured reflection coefficients for on-arm conditions of Antenna V.

Table 6: Frequency detuning of Antenna V for on-arm conditions.

On-arm condition	Frequency detuning (%)			
	1780 MHz	2.4 GHz	3.46 GHz	5.26 GHz
Without cloth	3.37	2.50	1.73	2.66
With cloth	2.24	1.66	1.15	1.90

detuning is observed at the 3.46 GHz band for the with-cloth condition.

Finally, we compare the proposed antenna with other wearable antennas having single-band [1, 2, 4, 5], dual-band [6–10], tri-band [11, 12], and quad-band [13] operations, and the results are listed in Table 7. The single-band wearable antennas in [1, 2] have comparatively lower SAR values at 2.4 GHz, but their sizes are larger than those of our proposed antenna. It can be seen that the sizes of the CPW-fed wearable antennas in [4–6, 8, 9] are smaller than those of our proposed four-band wearable antenna, but they are exhibiting only single-band and dual-band operations, respectively.

The gains of the dual-band wearable antennas in [7, 10] are better; however, their sizes are larger and their radiation efficiencies and bandwidths are lower than that of our proposed antenna. The gain, radiation efficiency, and SAR values of our proposed antenna are better than the tri-band wearable antennas proposed in [11, 12]. The quad-band wearable antenna in [13] has a larger size and lower bandwidths than that of the proposed antenna; however, its gain is higher for first, second, and fourth band, its radiation efficiencies are lower for the first three bands, and its SAR values are lower for the first two bands in comparison to the proposed antenna. The CPW line width of the proposed antenna is wider than the other works [4–6, 8, 9] illustrated in Table 7.

5. Conclusion

A novel wide CPW-fed multiband wearable monopole antenna and its design procedure have been proposed and successfully implemented. The antenna has a simple geometry and is easy to design on a polyester substrate. It has been shown that the proposed antenna with a wide CPW line is sufficient to cover the 1800 MHz GSM, 2.4/5.2 GHz WLAN, and 3.5 GHz WiMAX bands, resulting in a four-band operation. The antenna provides good radiation

Table 7: Comparison of the proposed antenna with existing literature.

Ref.	Size (mm^3)	Frequency (GHz)	BW (MHz/%)	Gain/directivity (dB or dBi)	Radiation efficiency (%)	SAR (W/kg)
[1]	$46 \times 46 \times 2.4$	2.4	660	7.8 dBi	—	0.0138
[2]	$100 \times 100 \times 3$	2.4	157	2.0 dB	45	0.0500
[4]	$50 \times 50 \times 1$	5.4	52.96%	9.67 dBi	—	—
[5]	$40 \times 40 \times 0.6$	5.7	—	6.49 dB	59	0.0043
[6]	$34.29 \times 48 \times 0.45$	2.45	458	3.9 dB	85	—
		5.8	590	4.6 dB	90	—
[7]	$240 \times 240 \times 1$	0.9	—	8.1 dBi	20.5	0.0011
		1.8	—	7.4 dBi	10.3	0.0034
[8]	$24 \times 32 \times 0.305$	5.2	4.07%	7.9 dB	90	0.0646
		5.8	4.16%	8.2 dB	90	0.0258
[9]	$31 \times 34 \times 0.0508$	2.46	648	1.68 dBi	91.6	—
		5.48	1378	1.64 dBi	91.6	—
[10]	$\pi \times (35)^2 \times 3$	2.45	84	4.16 dBi	63.5	0.248
		5.8	247	4.34 dBi	53	0.091
[11]	$105.5 \times 80.8 \times 0.015$	0.9	—		41.6	—
		1.9	—	2.0 dBi at all bands	75.8	—
		2.45	—		65.6	—
[12]	$40 \times 40 \times 0.8$	1.55	—			0.78
		1.95	—	>1.6 dB at all bands	>50 at all bands	0.62
		2.1	—			0.58
[13]	$70 \times 70 \times 2$	1.8	320	4.91 dBi	92.45	0.019
		2.4	60	7.84 dBi	75.22	0.358
		3.6	80	2.58 dBi	63.26	0.566
		5.5	180	4.12 dBi	88.95	0.798
Proposed antenna	$45.5 \times 85 \times 1$	1.78	410	4.17 dBi	94.71	0.2293
		2.40	260	3.81 dBi	93.42	0.3892
		3.46	170	2.60 dBi	90.52	0.4640
		5.26	520	2.74 dBi	83.97	0.2535

pattern characteristics and appreciable gain over each of the operating bands. The calculated SAR values at all the resonant frequencies of the wearable antenna are well below the acceptable limit of 2 W/kg, ensuring the safety of the user and viability of the proposed antenna for wearable applications. Further, the effect of bending in the x and y planes on antenna performance has been investigated and frequency detuning is discussed. Finally, the reflection coefficient characteristics has been measured for two on-arm conditions, with and without cloth, and the results are presented.

Data Availability

The data used to support the findings of this study are included within the article.

Conflicts of Interest

The authors declare that there is no conflict of interests regarding the publication of this paper.

Acknowledgments

We are thankful to I. K. Gujral Punjab Technical University, Jalandhar for providing the opportunity to do research and publish results.

References

[1] A. Y. I. Ashyap, Z. Zainal Abidin, S. H. Dahlan et al., "Compact and low-profile textile EBG-based antenna for wearable medical applications," *IEEE Antennas and Wireless Propagation Letters*, vol. 16, pp. 2550–2553, 2017.

[2] S. Yan and G. A. E. Vandenbosch, "Radiation pattern reconfigurable wearable antenna based on metamaterial structure," *IEEE Antennas and Wireless Propagation Letters*, vol. 15, pp. 1715–1718, 2016.

[3] J. G. Joshi, S. S. Pattnaik, and S. Devi, "Metamaterial embedded wearable rectangular microstrip patch antenna," *International Journal of Antennas and Propagation*, vol. 2012, Article ID 974315, 9 pages, 2012.

[4] P. J. Gogoi, S. Bhattacharyya, and N. S. Bhattacharya, "CPW-fed body worn monopole antenna on magneto-dielectric substrate

in C-band," *Progress In Electromagnetics Research C*, vol. 84, pp. 201–213, 2018.

[5] M. I. Ahmed, M. F. Ahmed, and A. E. H. Shaalan, "Novel electro-textile patch antenna on jeans substrate for wearable applications," *Progress In Electromagnetics Research C*, vol. 83, pp. 255–265, 2018.

[6] M. E. De Cos and F. Las-Heras, "Polypropylene-based dual-band CPW-fed monopole antenna (antenna applications corner)," *IEEE Antennas and Propagation Magazine*, vol. 55, no. 3, pp. 264–273, 2013.

[7] E. F. Sundarsingh, S. Velan, M. Kanagasabai, A. K. Sarma, C. Raviteja, and M. G. N. Alsath, "Polygon-shaped slotted dual-band antenna for wearable applications," *IEEE Antennas and Wireless Propagation Letters*, vol. 13, pp. 611–614, 2014.

[8] H.-L. Yang, W. Yao, Y. Yi, X. Huang, S. Wu, and B. Xiao, "A dual-band low-profile metasurface-enabled wearable antenna for WLAN devices," *Progress In Electromagnetics Research C*, vol. 61, pp. 115–125, 2016.

[9] H. K. Raad, H. M. Al-Rizzo, A. I. Abbosh, and A. I. Hammoodi, "A compact dual band polyimide based antenna for wearable and flexible telemedicine devices," *Progress In Electromagnetics Research C*, vol. 63, pp. 153–161, 2016.

[10] R. B. V. B. Simorangkir, Y. Yang, L. Matekovits, and K. P. Esselle, "Dual-band dual-mode textile antenna on PDMS substrate for body-centric communications," *IEEE Antennas and Wireless Propagation Letters*, vol. 16, pp. 677–680, 2017.

[11] Z. Wang, L. Z. Lee, D. Psychoudakis, and J. L. Volakis, "Embroidered multiband body-worn antenna for GSM/PCS/WLAN communications," *IEEE Transactions on Antennas and Propagation*, vol. 62, no. 6, pp. 3321–3329, 2014.

[12] B. Liu, J. Han, S. Hu, and L. Zhang, "Novel multiband metal-rimmed antenna for wearable applications," *International Journal of Antennas and Propagation*, vol. 2015, Article ID 319894, 7 pages, 2015.

[13] D. Mandal and S. S. Pattnaik, "Quad-band wearable slot antenna with low SAR values for 1.8 GHz DCS, 2.4 GHz WLAN and 3.6/5.5 GHz WiMAX applications," *Progress In Electromagnetics Research B*, vol. 81, pp. 163–182, 2018.

[14] Q. X. Chu and L. H. Ye, "Design of compact dual-wideband antenna with assembled monopoles," *IEEE Transactions on Antennas and Propagation*, vol. 58, no. 12, pp. 4063–4066, 2010.

[15] H. D. Chen and H. T. Chen, "A CPW-fed dual-frequency monopole antenna," *IEEE Transactions on Antennas and Propagation*, vol. 52, no. 4, pp. 978–982, 2004.

[16] H. D. Chen, "Compact CPW-fed dual-frequency monopole antenna," *Electronics Letters*, vol. 38, no. 25, pp. 1622–1624, 2002.

[17] M. T. Wu and M. L. Chuang, "Multibroadband slotted bow-tie monopole antenna," *IEEE Antennas and Wireless Propagation Letters*, vol. 14, pp. 887–890, 2015.

[18] S. Jo, H. Choi, J. Lim, B. Shin, S. Oh, and J. Lee, "A CPW-fed monopole antenna with double rectangular rings and vertical slots in the ground plane for WLAN/WiMAX applications," *International Journal of Antennas and Propagation*, vol. 2015, Article ID 165270, 7 pages, 2015.

[19] H. W. Liu, C. H. Ku, and C. F. Yang, "Novel CPW-fed planar monopole antenna for WiMAX/WLAN applications," *IEEE Antennas and Wireless Propagation Letters*, vol. 9, pp. 240–243, 2010.

[20] A. Lak and H. Oraizi, "Evaluation of SAR distribution in six-layer human head model," *International Journal of Antennas and Propagation*, vol. 2013, Article ID 580872, 8 pages, 2013.

[21] J. Gemio, J. Parron, and J. Soler, "Human body effects on implantable antennas for ISM bands applications: models comparison and propagation losses study," *Progress In Electromagnetics Research*, vol. 110, pp. 437–452, 2010.

[22] M. Klemm and G. Troester, "EM energy absorption in the human body tissues due to UWB antennas," *Progress In Electromagnetics Research*, vol. 62, pp. 261–280, 2006.

[23] O. Kivekas, T. Lehtiniemi, and P. Vainikainen, "On the general energy absorption mechanism in the human tissue," *Microwave and Optical Technology Letters*, vol. 43, no. 3, pp. 195–201, 2004.

[24] B. Hu, G. P. Gao, L. L. He, X. D. Cong, and J. N. Zhao, "Bending and on-arm effects on a wearable antenna for 2.45 GHz body area network," *IEEE Antennas and Wireless Propagation Letters*, vol. 15, pp. 378–381, 2016.

[25] R. N. Simons, *Coplanar Waveguide Circuits, Components, and Systems*, John Wiley & Sons, 2001.

[26] FCC, "Body tissue dielectric parameters," https://www.fcc.gov/oet/rfsafety/dielectric.html.

[27] M. M. Weiner, *Monopole Antennas*, Marcel Dekker, 2003.